Electromagnetic wave absorption characteristics of H-shaped fractal antenna for dual-band microbolometer and study on the influence of bias line resistivity on microbolometer characteristics

Kozaburo Takebe[1], Hidetoshi Miyashita[1], Keisuke Takano[2], Masanori Hangyo[2], Sang-Seok Lee[1]

[1]*Graduate School of Engineering, Tottori University, Tottori 680-8552, Japan*
[2]*Institute of Laser Engineering, Osaka University, Suita 565-0871, Japan*
E-mail: sslee@ele.tottori-u.ac.jp

Published in Micro & Nano Letters; Received on 15th May 2014; Revised on 14th July 2014; Accepted on 30th July 2014

A dual-band microbolometer coupled with an H-shaped fractal antenna, which can detect both infrared (IR) and THz waves simultaneously is proposed. Firstly, the H-shaped fractal antenna for 125 and 500 μm dual-bands is proposed by using the dipole antenna formula and finite element method (FEM) simulation. On the basis of simulation results, the H-shaped fractal antenna for the microbolometer is fabricated and the electromagnetic wave absorption characteristics of it are measured. Transmission measurement successfully confirmed the absorption peaks near the aimed for two wavelengths in the IR and THz regions, respectively. It showed that the proposed microbolometer coupled with the H-shaped fractal antenna is considered as a useful tool for widely separated multi-band detection. Moreover, for the microbolometer design, the influence of bias line resistivity on microbolometer characteristics with two different bias line materials by the FEM simulation is studied. It is observed that the electromagnetic wave absorption characteristics of the microbolometer are affected by the resistivity of the bias line material, especially when the parallel polarised incident wave to the bias line formation direction is irradiated.

1. Introduction: Since antenna coupled microbolometers have many advantages such as fast response time, low power consumption and the detectivity of the electromagnetic wave over wide frequency ranges [1, 2], they have attracted a lot of attention. Moreover, antenna coupled microbolometers can be fabricated easily compared with other uncooled infrared (IR) or THz sensors because generally they have monolithic structures that can be fabricated using standard integrated circuit manufacturing techniques such as lithography, thin film deposition and etching. The antenna coupled microbolometers detect the aimed for electromagnetic wave by an antenna and the resonated electromagnetic wave is transformed to thermal energy, which causes the electrical resistive variation (shift) of the microbolometer material. By applying a constant current through the microbolometer material, one can measure a change in the bias voltage of the microbolometer, which indicates a change in temperature.

Fractal structures have potential for various applications. Among them, we focus on their application to antennas because they can resonate to multi-frequencies [3, 4]. As an example of fractal antenna application especially in the THz range, the emission characteristics of the H-shaped fractal antenna were investigated and multi-frequency emission peaks were reported [5].

In this Letter, we propose an antenna coupled microbolometer utilising the H-shaped fractal antenna to achieve widely separated dual-band detection ranging from IR to THz frequencies. The schematic diagram of our proposed microbolometer is shown in Fig. 1. Our device mainly consists of the H-shaped fractal antenna, a VO_x layer as a microbolometer material and the bias line to apply a constant current. Etching holes are formed for Si substrate removal, which is for thermal isolation. To show the whole device structure, the SiO_2 layer is lifted up in Fig. 1.

The H-shaped fractal antenna is designed by simulation and fabricated by the electron beam lithography technique. In this Letter, we first report the design results of the H-shaped fractal antenna for dual-band detection. Furthermore, we report the measured electromagnetic wave absorption characteristic results for our H-shaped fractal antenna fabricated to verify dual-band sensitivity, which will be compared and discussed with the simulation results. Finally, the investigation results of the bias line resistivity effect on the electromagnetic wave absorption characteristics will be discussed to estimate our microbolometer characteristics as well.

2. Design and simulation: To verify the dual-band sensitivity of our proposed microbolometer shown in Fig. 1, we designed the H-shaped fractal antenna to resonate at two different wavelengths of 125 and 500 μm. First, we determined the dimensions of the H-shaped fractal antenna resonating at these two wavelengths by the simulation. A schematic simulation model of the H-shaped fractal antenna is shown in Fig. 2. An H-shaped fractal antenna is formed on Si substrate with a 200 nm-thick SiO_2 layer. The material of the antenna is Au. The width (W) and thickness of the H-shaped fractal antenna are fixed as 2 and 0.1 μm, respectively. Lastly, we determined the lengths L_1 and L_2 of the H-shaped fractal antenna in Fig. 2, which are given by the target resonant wavelengths of the microbolometer. To determine antenna lengths L_1 and L_2, we used the dipole antenna formula

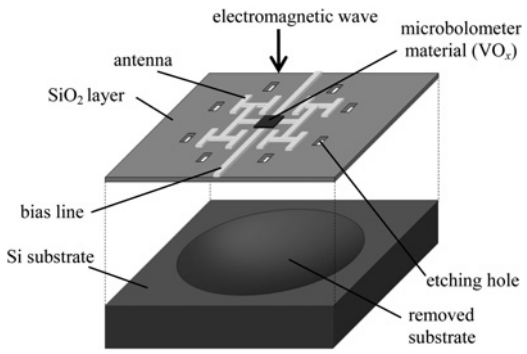

Figure 1 *Schematic diagram of an H-shaped fractal antenna coupled dual-band microbolometer*
SiO_2 layer is lifted up to show removed substrate structure beneath the SiO_2 layer

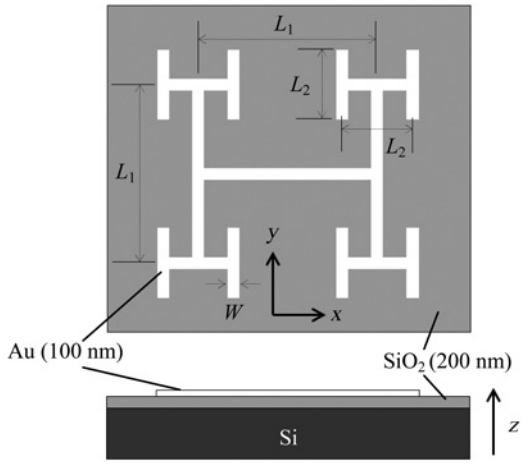

Figure 2 *Simulation model of an H-shaped fractal antenna of dual-band microbolometer*
W (=2 μm) and L_1, L_2 represent antenna width and lengths, respectively

[6, 7] for the conventional dipole antenna design as follows

$$L = \frac{0.48A}{\sqrt{\varepsilon_e}}\lambda \tag{1}$$

where λ is the wavelength, L is the dipole antenna length, which resonates at wavelength λ, $A = (1/(1 + W/L))$, W (=2 μm) is the antenna width, $\varepsilon_e = (1 + \varepsilon_r)/2$ and ε_r (=11.669) is the relative permittivity of the Si substrate, respectively. The antenna lengths L_1 and L_2 calculated from formula (1) for the aimed for two wavelengths resulted as being 93.4 and 21.8 μm, respectively. With these dimensions, the absorption spectrum (resistive loss) for the *x*-polarised electromagnetic irradiation of 1 V/m from the +*z*-direction was calculated by finite element method (FEM) simulation to confirm the antenna performance. The resistive loss means the total amount of thermal dissipation of the antenna caused by Joule heat, which is induced by electromagnetic wave resonance. In other words, the peaks of the resistive loss appear at the resonance wavelengths. As a simulation tool, we utilised COMSOL Multiphysics simulation package. In the simulation, to obtain an accurate result the length of a side of a mesh element is kept less than 0.1 × (incident wavelength) × (relative permittivity of the material to be meshed)$^{-1/2}$.

The simulated resistive loss is shown in Fig. 3. The resonant wavelengths are located at about 250 and 1363 μm, respectively. In Fig. 3 we call the longer side and the shorter side resonance mode mode 1 and mode 2, respectively. As the H-shaped fractal antenna consists of the connection of dipole antennas, the resonant

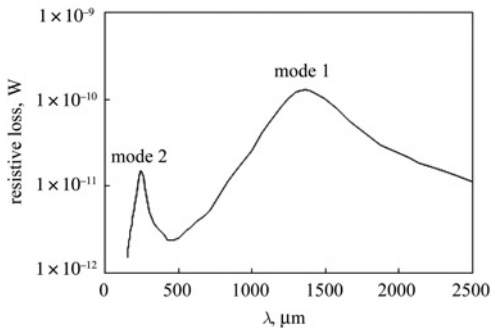

Figure 3 *Simulated resistive loss for the x-polarised incidence from the +z-direction*
Antenna lengths L_1, L_2 and width *W* are 93.4, 21.8 and 2 μm, respectively

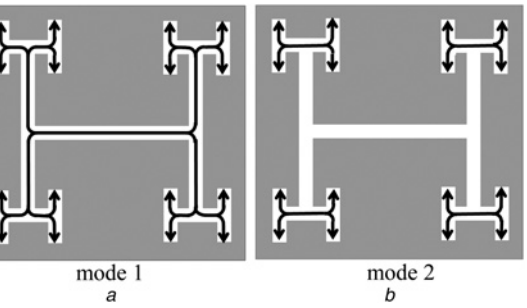

Figure 4 *Schematic diagrams of the current paths (black arrowed lines) at each resonant wavelength, where mode 1 and mode 2 represent current paths of longer side and shorter side resonant wavelengths, respectively*
a Mode 1
b Mode 2

wavelengths were shifted largely to the longer wavelength side than the objective wavelengths although we were able to confirm the dual-band sensitivity of it. To correct antenna dimensions, we investigated current paths at the resonant wavelengths by FEM simulation. The current paths obtained by FEM simulation are represented in Fig. 4, by which we could confirm two resonance modes corresponding to two resonant wavelengths. As shown in mode 1 corresponding to the resonant wavelength of 1363 μm, the current flows in both L_1 and L_2, namely the current path length becomes $2(L_1 + L_2)$. On the other hand, in the case of mode 2 corresponding to the resonant wavelength of 250 μm, mainly the current flows in the small H-shaped antenna consisted of L_2s, namely the current path length becomes $2L_2$. We equalised current path lengths corresponding to mode 1 and mode 2 to the calculated antenna lengths given by the dipole antenna formula (1), that is $2(L_1 + L_2)$ and $2L_2$ are modified to 93.4 and 21.8 μm, respectively.

As the results of recalculation, we obtained antenna lengths of $L_1 = 35.8$ μm and $L_2 = 10.9$ μm, respectively. Again, we calculated the absorption spectrum for these antenna lengths by FEM simulation, and the result is shown as the dashed line in Fig. 5. The resonant wavelengths are still shifted a little from the designed values of 125 and 500 μm. Note that the obtained resonant wavelengths by the simulation are 115 and 545 μm. It seems that the shifts were caused by the parasitic capacitance of the antenna. Especially in case of the longer side resonant wavelength shift, its influence seems to be relevant. Therefore, it is necessary to adjust the length of shorter L_1. As a result of adjusting the antenna lengths to be resonated at 125 and 500 μm by FEM simulation, the antenna lengths were determined to be 30 and 11.8 μm for L_1 and L_2, respectively.

The simulation result of the absorption spectrum with finally adjusted lengths is shown as the solid line in Fig. 5. The resonant wavelengths are located at 125 and 491 μm for the *x*-polarised

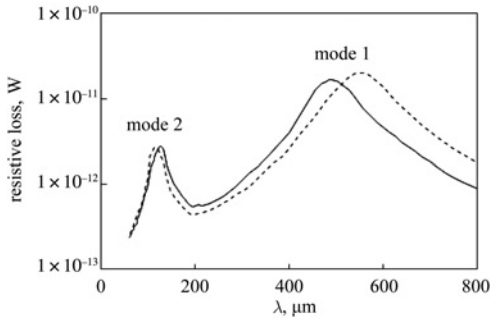

Figure 5 *Simulated resistive losses for the x-polarised incidence from the +z-direction to the antennas having the dimensions of $L_1 = 35.8$ μm and $L_2 = 10.9$ μm (dashed line), and $L_1 = 30$ μm and $L_2 = 11.8$ μm (solid line), respectively*

doi: 10.1049/mnl.2014.0266

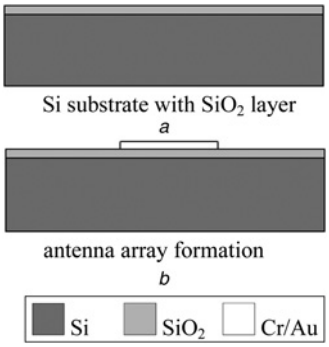

Figure 6 *Fabrication process flow of the H-shaped fractal antenna array*
a Si substrate with SiO_2 layer
b Antenna array formation

incident electromagnetic wave. The resistive loss at mode 2 is smaller than that of mode 1. It means that the excited current at mode 2 is smaller than that of mode 1.

3. Fabrication: We fabricated the H-shaped fractal antenna to verify its dual-band sensitivity according to the design results in Section 2. The fabrication process of our H-shaped fractal antenna is illustrated in Fig. 6. In this study, we fabricated two-dimensional arrays of the H-shaped fractal antenna to observe the resonant wavelengths easily. On the Si substrate with a 200 nm-thick SiO_2 layer (Fig. 6*a*), the array of the antenna element and the bias line were patterned using the electron-beam (EB) lithography technique and the lift-off process (Fig. 6*b*). The antenna element was patterned with 50 μm pitch in a 5 mm^2 area. The metal layers of the antenna consist of 50/100 nm-thick Cr/Au layers. The SEM image of the fabricated H-shaped fractal antenna array is shown in Fig. 7.

4. Measurement results and discussion: We measured the transmittance with our fabricated H-shaped fractal antenna array to confirm dual-band sensitivity and our simulation results. The transmittance was measured by Fourier transform infrared spectroscopy (FTIR) and terahertz time-domain spectroscopy (THz-TDS) methods. The measurement results are shown in Fig. 8, where the solid line and the dashed line represent the transmission spectra measured by FTIR and THz-TDS, respectively, with the *x*-polarised incidence from the +*z*-direction to verify the resonance at the wavelength of 125 and 500 μm, respectively. The dips of transmittance exist at about 110 and 512 μm. The sharp peak appeared at about 119 μm in the FTIR measurement result is because of noise. The wavelengths of the dips in the transmission measurement results and that of the peaks in the resistive loss simulation results should coincide. Consequently, we were able to confirm the dual-band sensitivity of our H-shaped fractal antenna array by the experiment.

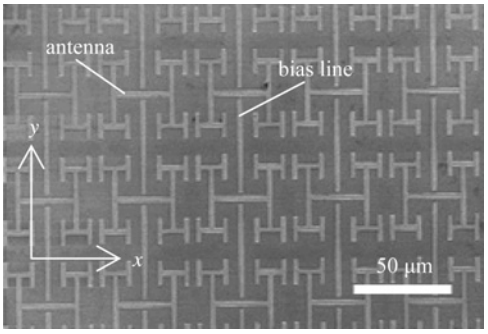

Figure 7 *SEM image of the fabricated H-shaped fractal antenna array*

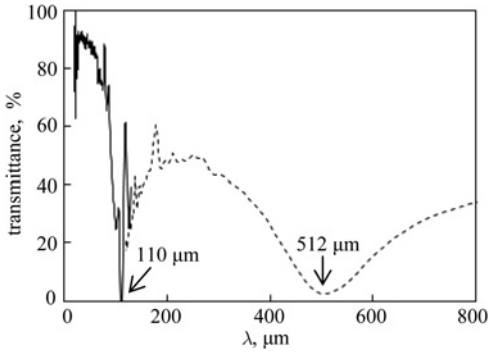

Figure 8 *Measured transmittance spectra for the x-polarised incidence from the +z-direction*
Solid and dashed lines are measurement results by FTIR and THz-TDS, respectively

However, there are slight differences between the final simulation results in Fig. 5 and the experimental results in Fig. 8.

We modified our simulation model to obtain more accurate simulation results. First, we checked the fabricated antenna dimensions, and found that they were different from the designed dimensions. These differences may have been caused by differences between the formed photoresist pattern dimensions and the mask dimensions that occurred in the electron beam lithography process. The modified simulation model according to the measured dimensions is represented in Fig. 9 and we call it model A. With the modified simulation model A, we simulated again the resistive loss. The simulation result is shown in Fig. 10. We obtained the resonant wavelengths of 136 and 504 μm. The simulation result of the longer side resonant wavelength of 504 μm is almost the same as the measurement result. However, in the case of the resonant wavelength of the

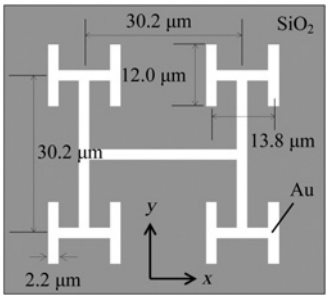

Figure 9 *Modified simulation model according to measured dimensions of a fabricated the H-shaped fractal antenna in the antenna array (called model A)*

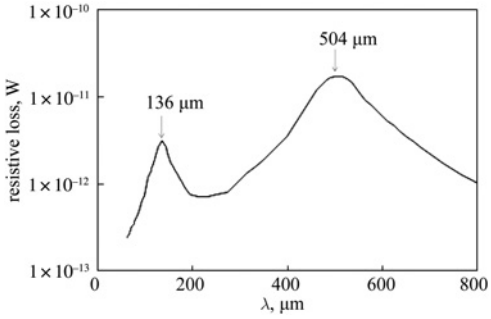

Figure 10 *Simulated resistive loss for the x-polarised incidence from the +z-direction with modified simulation model A, whose dimensions are given by fabricated antenna*

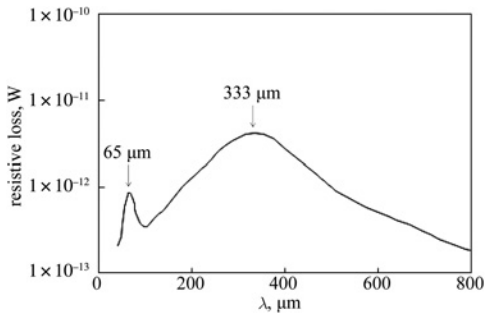

Figure 11 *Simulated resistive loss for the y-polarised incidence from the +z-direction with modified simulation model A, whose dimensions are given by fabricated antenna*

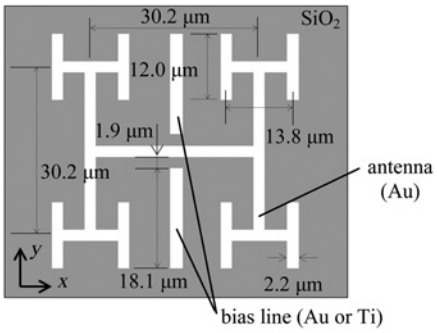

Figure 13 *Simulation model of a fabricated H-shaped fractal antenna with measured dimensions and bias lines*
Bias line material is considered as Au (called model B) or Ti (called model C)

shorter wavelength side, there still exist differences between the measurement and simulation values. This disagreement may have been caused by the difference in structure between the simulation model, which has only one antenna element, and that of the measured antenna, which has the array of antennas and bias lines.

We also investigated the electromagnetic absorption characteristics of the H-shaped fractal antenna for the *y*-polarised incidence from the +*z*-direction. The simulation result of the absorption spectrum (resistive loss) for the *y*-polarised incidence is shown in Fig. 11. The resonant wavelengths are located at 65 and 333 μm. The measurement results of the transmittance of the fabricated H-shaped fractal antenna array with the *y*-polarised incidence are shown in Fig. 12, in which the solid line and dashed line represent the transmission spectra measured by FTIR and THz-TDS, respectively. The sharp peaks that appear in the FTIR measurement result are because of noise. The dips of transmittance exist at 48, 191 and 259 μm. Although the simulated resistive loss has only two resonant peaks, the transmittance has three dips. Moreover, the simulated resonant wavelengths are different to the wavelengths of the transmittance dips in the measurement results. This difference also may be caused by the difference of the structure between the simulation model and fabricated antenna. The two dips that appear in the longer resonant wavelength side in Fig. 12 are considered to be a result of the electromagnetically induced transparency-like phenomenon, which will be discussed in a separate paper.

In the microbolometer, a constant current is applied through bias lines to measure the resistance variation of the microbolometer material caused by electromagnetic wave absorption. To obtain a more accurate simulation model, we studied the influence of the bias line resistivity on the antenna and the microbolometer characteristics. To do so, we modified model A by addition of 18.1 μm-long, 100 nm-thick and 2.2 μm-wide two bias lines that are formed parallel to the

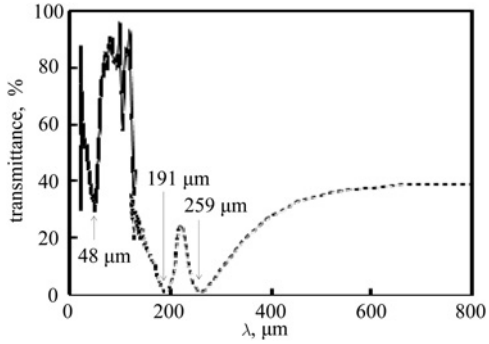

Figure 12 *Measured transmittance spectra for the y-polarised incidence from the +z-direction*
Solid and dashed lines are measurement results by FTIR and THz-TDS, respectively

y-axis. A modified simulation model having bias lines is represented in Fig. 13. In this study, we investigated two different bias line resistivities; one is the Au and another is the Ti bias line whose resistivity is about 18 times greater than that of Au. We call the modified models with the Au and Ti bias lines model B and model C, respectively.

The simulated resistive losses of models A, B and C for the *x*-polarised incidence from the +*z*-direction are shown in Fig. 14. Note that the simulation results for models B and C shown in Fig. 14*a* represent the resistive losses occurred only in the antenna. In other words, the resistive losses that occurred in the bias lines are excluded in the simulation results represented in Fig. 14*a* to investigate the bias line effect on the antenna characteristics. The results in Fig. 14*a* show that the resistive losses of the antenna portion for models B and C are hardly changed compared with that of model A. In addition, we investigated the total resistive

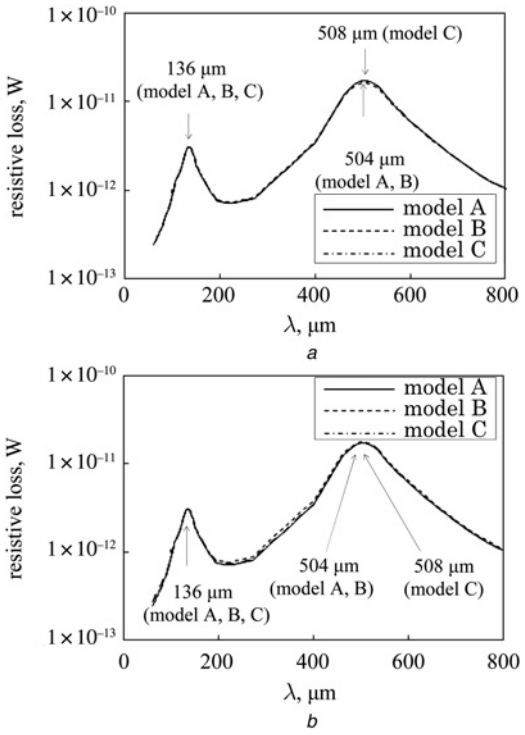

Figure 14 *Simulated resistive loss for the x-polarised incidence from the +z-direction*
a Resistive loss of each antenna for models A, B and C
b Resistive loss of the antenna for model A, and the sum of the resistive losses of antenna and bias line for models B and C
In each graph, wavelengths at peak for each model are indicated

doi: 10.1049/mnl.2014.0266

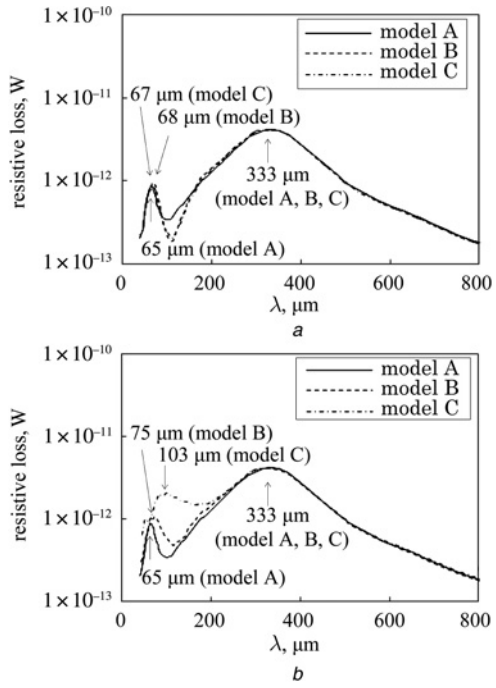

Figure 15 *Simulated resistive loss for the y-polarised incidence from the +-direction*
a Resistive loss of each antenna for models A, B and C
b Resistive loss of the antenna for model A, and the sum of the resistive losses of antenna and bias line for models B and C
In each graph, wavelengths at peak for each model are indicated

losses occurring in both the antenna and the bias lines for models B and C, for which the simulation results are represented in Fig. 14*b*. By the simulation results of Fig. 14*b*, we can estimate the influence of the bias line on the microbolometer characteristics because the resistive loss occurred in the bias line may contribute to the temperature increase of the microbolometer material such as VO_x, which will be in contact with the bias line for applying a constant current (see Fig. 1). As shown in Fig. 14*b*, the total resistive losses including the bias line portion of models B and C are also hardly changed compared with that of model A. As a result, we conclude that the bias line itself and its resistivity have almost no influence on both antenna and microbolometer characteristics when the incident electromagnetic wave is *x*-polarised.

Similarly, we studied the influence of the bias line itself and its resistivity on antenna and microbolometer characteristics for the *y*-polarised electromagnetic wave incidence, which is parallel with the bias line. The investigation results are shown in Fig. 15 for models A, B and C. The simulated resistive losses of the antenna only and the total resistive losses including the bias line portion for each model are represented and compared in Figs. 15*a* and *b*, respectively. Although the resistive losses of models B and C around from 70 to 200 μm in Fig. 15*a* are slightly smaller than that of model A, the peak wavelengths and the peak intensities of these models are almost the same. On the other hand, the peak wavelengths and the peak intensities of the total resistive losses including the bias line portion for models B and C shown in Fig. 15*b* are different from that for model A. It seems that these behaviours resulted from the influence of the resistive losses of the bias lines in models B and C because of resonance at from 70 to 200 μm for the *y*-polarised incident electromagnetic wave. Furthermore, the resistive loss difference caused by bias line resonance between models B and C came from the resistivity difference of the bias line materials. Note that the resistivity of Ti is about 18 times greater than that of Au, and the influence of bias line resistive loss in model C is greater than that in model B. In the case when the incident electromagnetic wave is *y*-polarised, we have to consider the influence of resistive loss occurring in the bias line in the design process for the antenna coupled microbolometer.

5. Conclusions: We have proposed a dual-band microbolometer coupled with an H-shaped fractal antenna, which can detect both IR and THz waves simultaneously. Firstly, we designed the H-shaped fractal antenna by using the dipole antenna formula and FEM simulation, which has two resonance wavelengths of 125 and 500 μm.

To verify the widely separated dual-band sensitivity of our designed H-shaped fractal antenna, we fabricated the H-shaped fractal antenna and measured its characteristics for the *x*-polarised incidence.

As a result of transmission measurement, we can confirm the absorption peaks near the aimed for two wavelengths in the IR and THz regions, respectively. This shows that our microbolometer coupled with the H-shaped fractal antenna can be considered as a useful tool for widely separated multi-bands detection.

Furthermore, we investigated the characteristics of the H-shaped fractal antenna for the *y*-polarised incidence by FEM simulation and measurement. Their resonant wavelengths were different to those for the *x*-polarised incidence and we have found a peculiar phenomenon, which will be discussed elsewhere. If we utilise both the *x*- and *y*-polarised wave as incidence waves, the selectivity of detectable wavelengths will be enhanced.

Lastly, we investigated the bias line effect on the antenna and microbolometer characteristics with two different bias line materials. The simulation results show that the influence of the bias line itself and its resistivity on the antenna characteristics for both *x*- and *y*-polarised incidence is not remarkable. However, it affects the characteristics of the microbolometer, especially for the *y*-polarised incidence, and therefore it is necessary to take account of the bias line resistivity in the design process when the microbolometer is used for the *y*-polarised incidence.

6. Acknowledgments: A part of this work was supported by the Kyoto University Nano Technology Hub in the 'Nanotechnology Platform Project' sponsored by the Ministry of Education, Culture, Sports, Science and Technology (MEXT), Japan.

7 References

[1] Gonzalez F.J., Ashley C.S., Clem P.G., Boreman G.D.: 'Antenna-coupled microbolometer arrays with aerogel thermal isolation', *Infrared Phys. Technol.*, 2004, **45**, pp. 47–51
[2] Middletona C.F., Boreman G.D.: 'Technique for thermal isolation of antenna-coupled infrared microbolometers', *J. Vac. Sci. Technol. B*, 2006, **24**, pp. 2356–2359
[3] Werner D.H., Haupt R.L., Werner P.L.: 'Fractal antenna engineering: the theory and design of fractal antenna arrays', *IEEE Antennas Propag. Mag.*, 1999, **41**, pp. 37–59
[4] Miyamaru F., Saito Y., Takeda M.W., *ET AL.*: 'Terahertz electric response of fractal metamaterial structures', *Phys. Rev. B*, 2008, **77**, p. 045124
[5] Miyamaru F., Saito Y., Takeda M.W., Hou B., Wen W., Sheng P.: 'Characteristics of terahertz radiation emitted from fractal photoconductive antennas', *Jpn. J. Appl. Phys.*, 2010, **49**, p. 070205
[6] Hiromoto N., Aoki M., Takeda M.: 'Comparison between antenna-coupled and infrared-type microbolomters for room-temperature THz detection'. Proc. Int. Symp. on Frontiers in THz Tech. (FTT 2012), Pos1.29, Nara, Japan, 2012, **5**
[7] Kominami M., Pozar D.M., Schaubert D.H.: 'Dipole and slot elements and arrays on semi-infinite substrates', *IEEE Trans. Antenna Propag.*, 1985, **33**, pp. 600–607